



# A Composite Fe–V/g-C<sub>3</sub>N<sub>4</sub> for Liquid-Phase Selective Oxidation of Methanol with O<sub>2</sub> Oxidant

Jing Zhang<sup>1</sup> · Hongxia Wang<sup>1</sup> · Bin Lu<sup>1</sup> · Jingxiang Zhao<sup>1</sup> · Qinghai Cai<sup>1</sup>

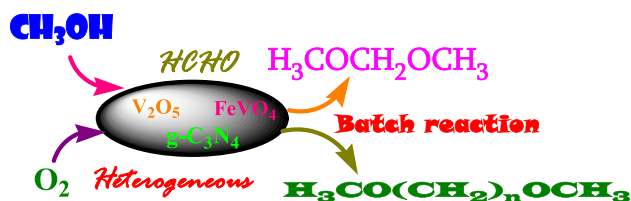
Received: 16 June 2020 / Accepted: 7 August 2020  
© Springer Science+Business Media, LLC, part of Springer Nature 2020

## Abstract

A composite material Fe–V/g-C<sub>3</sub>N<sub>4</sub> prepared by impregnation achieved an efficient performance for heterogeneously catalytic oxidation of methanol to dimethoxymethane (DMM) and poly(oxymethylene) dimethyl ethers (POM) by O<sub>2</sub> oxidant in batch reactor, exhibiting 34.3% conversion and > 99.0% selectivity to DMM and POM. However, a pioneered strategy for tuneable synthesis of DMM and POM was realized by controlling the reaction time. The experimental results revealed that FeVO<sub>4</sub> and V<sub>2</sub>O<sub>5</sub> nanoparticle crystallizes served as the active sites and higher specific areas 29.3–51.9 m<sup>2</sup>/g for the catalysts were jointly responsible for the high activity. Besides, the catalyst could be easily recovered and effectively reused.

## Graphic Abstract

A composite material Fe–V/g-C<sub>3</sub>N<sub>4</sub> with higher specific area exhibited efficient performance for heterogeneously catalytic oxidation of methanol to dimethoxymethane (DMM) and polyoxymethylene dimethyl ether (POM) in batch reactor using O<sub>2</sub> oxidant. Moreover, a pioneered strategy for tunable synthesis of DMM and POM was realized by controlling the reaction time. The catalyst was easily recovered and had excellent recycle lifetime and stability.



**Keywords** Composite Fe–V/g-C<sub>3</sub>N<sub>4</sub> · Methanol · Dimethoxymethane · Liquid-phase oxidation · Heterogeneous catalysis

**Electronic supplementary material** The online version of this article (<https://doi.org/10.1007/s10562-020-03354-1>) contains supplementary material, which is available to authorized users.

- ✉ Bin Lu  
lupin630411@163.com
- ✉ Qinghai Cai  
caiqinghai@yahoo.com

<sup>1</sup> Key Lab for Photonic and Electronic Bandgap Materials, Ministry of Education, School of Chemistry and Chemical Engineering, Harbin Normal University, No. 1 Shida Road Limin Development Zone, Harbin 150025, People's Republic of China

## 1 Introduction

The selective oxidation of alcohols is one of the most important functionalized group transformations in organic synthesis due to producing valuable oxo-compounds involving aldehydes, carboxylic acid and esters. As a simplest alcohol, methanol can be selectively oxidized into formaldehyde (FA), formic acid and other products such as methyl formate and dimethoxymethane (DMM), or a polymer of DMM, polyoxymethylene dimethyl ether [1]. Among them, DMM is a versatile chemical intermediate widely used for producing perfume, pharmaceuticals, dyestuff and agrochemicals due to low toxicity [2], as well as for preparing high concentration formaldehyde (highest concentration approaching to 83.3%) [3], which is advantageous to production of

polyformaldehyde, a kind of engineering plastics. Besides, DMM or its polymer POM, is found to be a more potential additive for diesel fuels because of their high oxygen content and cetane number [4, 5], and thus the demand for DMM may be considerably increased. Since the traditional method for synthesizing DMM by the condensation of FA with methanol over acidic catalysts [6] has some demerits, for example, equipment corrosion caused by acidic catalysts, impediment role of massive water in raw formaldehyde solution for the condensation, which results in intricate and costly. Consequently, one-step selective oxidation of methanol into DMM has been widely attempted. There are numerous catalysts such as  $\text{Re}/\gamma\text{-Fe}_2\text{O}_3$  [7],  $\text{RuO}_x/\text{SiO}_2$  [8],  $\text{SbRe}_2\text{O}_6$  [9, 10],  $\text{SO}_4^{2-}/\text{V}_2\text{O}_5\text{-TiO}_2$  [11] and  $\text{VO}_x/\text{TS-1}$  [12], etc. that have been reported to be active for one-step methanol oxidation. Recently, our group has addressed  $\text{VO}_x$  supported catalysts,  $\text{SO}_4^{2-}/\text{V}_2\text{O}_5\text{-ZrO}_2$  and  $\text{VO}_x/\text{g-C}_3\text{N}_4$  [13, 14], that presented higher activity and high selectivity to DMM. However, these two catalysts are apt to deactivation after reaction having carried out for 9 h at 200 °C. Nevertheless, all the above reported processes have performed in fixed-bed reactor, in which over-oxidation of methanol into  $\text{CO}_2$  usually occurs due to high reaction temperature [1]. The liquid-phase oxidation of methanol to DMM has been very rare in reported literatures [13]. Li et al. have demonstrated effective catalytic performance of ruthenium trichloride for homogeneously catalytic oxidation of methanol using  $\text{O}_2$  as oxidant [15], getting good reactivity. Herein, the aim of this study is to design and develop an efficient solid catalyst for liquid-phase oxidation of methanol in heterogeneous catalysis. A composite material  $\text{Fe-V/g-C}_3\text{N}_4$  with higher specific area was prepared in order to modify the  $\text{VO}_x/\text{g-C}_3\text{N}_4$  catalyst via introducing iron species. The catalytic performance upon the relationship between the surface composition, structure and the activity of the composite catalyst, the role of the Fe species for promoting the catalytic activity and reusability of the catalyst were thus evaluated. The experiment results on oxidation of methanol into DMM and POM were discussed in this paper.

## 2 Experimental

### 2.1 Preparation of the Catalyst

$\text{g-C}_3\text{N}_4$  was prepared via melamine precursor according to the method described in the literature [14].

A typical preparation of composite material  $\text{Fe-V/g-C}_3\text{N}_4$ , 1.4 g (10.53 mmol) of  $\text{NH}_4\text{VO}_3$  (> 99.0%) and 100 mL of distilled water were added into a beaker. The suspension was stirred and heated to 60 °C for dissolving  $\text{NH}_4\text{VO}_3$ . After the dissolution, 2.0 g of  $\text{g-C}_3\text{N}_4$  and 2.0 g (7.39 mmol) of  $\text{FeCl}_3\cdot 6\text{H}_2\text{O}$  were charged to the beaker, followed by

stirring at this temperature for 6 h. Afterwards, a dark green solid was filtered off and dried at 100 °C for 2 h. Finally, the solid was grinded into powder and calcined at 550 °C for 2 h, affording  $\text{Fe-V/g-C}_3\text{N}_4$  (1.62 g) with content of Fe 19.8%, V 24.3%. For convenience, the composite materials by calcined at 400, 450, 500, 550 and 600 °C were marked as  $\text{Fe-V/g-C}_3\text{N}_4\text{-400}$ ,  $\text{Fe-V/g-C}_3\text{N}_4\text{-450}$ ,  $\text{Fe-V/g-C}_3\text{N}_4\text{-500}$ ,  $\text{Fe-V/g-C}_3\text{N}_4\text{-550}$  and  $\text{Fe-V/g-C}_3\text{N}_4\text{-600}$ , respectively.

### 2.2 Characterization

X-ray powder diffraction (XRD) of the composite materials was performed with a Bruker AXS D8 advanced X-ray diffractometer. SEM, SEM-EDX and the EDX elemental mapping were obtained with a Hitachi S-4800 scanning electron microscopy. FT-IR spectra were recorded on a Vertax-80 spectrometer. TEM and HRTEM were carried out using a FEI Tecnai F20 equipment. X-ray photoelectron spectroscopy (XPS) was measured on a Kratos-AXIS ULTRA DLDX X-ray photoelectron spectrometer. Vanadium and iron contents in  $\text{Fe-V/g-C}_3\text{N}_4$  composite were analyzed by 7500CE ICP-MS (Agilent Company).

### 2.3 Catalytic Test

Test for catalytic activity of  $\text{Fe-V/g-C}_3\text{N}_4$  was conducted in a 100 mL stainless steel autoclave with an electric heater and a mechanical stirrer. 20 mL (0.494 mol) of methanol and 0.2 g of the catalyst ( $\text{Fe-V/g-C}_3\text{N}_4$ ) were loaded into the autoclave. After purged three times with  $\text{O}_2$  gas, the reactor was pressured to an initial pressure of 1 MPa  $\text{O}_2$  and heated to 175 °C; and then the reaction mixture was violently stirred at this temperature for 6 h. After the reaction completed, the reaction mixture was cooled down and filtered to separate the catalyst. The filtrate was analyzed by GC (Agilent GC7820) and GC-MS (Agilent GC7890A-MS5975C) using HP-5 column (30 m  $\times$  0.32 mm  $\times$  0.25  $\mu\text{m}$ ) and FID detector (GC). The separated catalyst was dried at 100 °C for 3 h, and then reused in the next run to evaluate the reusability of the catalyst. The lifetime of the catalyst was also evaluated in a fixed bed reactor at pressure 0.2 MPa and the other reaction conditions were the same as the description in the reference [14]. In addition, the selectivity to POM was also estimated by weighing the remnants after distillation to remove the methanol and DMM.

## 3 Results and Discussion

### 3.1 Characterization

XRD patterns of the prepared  $\text{g-C}_3\text{N}_4$  and  $\text{Fe-V/g-C}_3\text{N}_4\text{-t}$  materials (t = 400, 450, 500, 550 and 600, respectively)

were depicted in Fig. 1. The strong peaks at  $2\theta = 27.5$  and  $13.1^\circ$  indexed to (002) and (100) diffraction planes of the graphite-like carbon nitride (g-C<sub>3</sub>N<sub>4</sub>) [16] were observed (Fig. 1a). The peak at  $2\theta = 13.1^\circ$  could be ascribed to an in-plane structure motif, such as the hole to hole distance of tri-s-triazine units, while the peak at  $2\theta = 27.5^\circ$  was derived from the stacked interlayers of g-C<sub>3</sub>N<sub>4</sub> [17]. When Fe and V elements were incorporated, the diffraction peaks at the (002) plane were sharply decreased and shifted for Fe-V/g-C<sub>3</sub>N<sub>4</sub>-400 and Fe-V/g-C<sub>3</sub>N<sub>4</sub>-450 (Fig. 1b, c), and almost disappeared for Fe-V/g-C<sub>3</sub>N<sub>4</sub>-500 (Fig. 1d). While, the diffraction peaks at  $13.1^\circ$  related to the (100) plane were obviously changed to be weaker and wider for Fe-V/g-C<sub>3</sub>N<sub>4</sub>-400, Fe-V/g-C<sub>3</sub>N<sub>4</sub>-450 and Fe-V/g-C<sub>3</sub>N<sub>4</sub>-500, implying that the Fe and V species could reduce the crystalline degree and shift diffraction peak of the g-C<sub>3</sub>N<sub>4</sub> via interacting with its surface functional groups on in-plane structure motif and the stacked interlayers of g-C<sub>3</sub>N<sub>4</sub>. Interestingly, the sharp diffraction peaks at  $2\theta = 15.6^\circ$ ,  $20.5^\circ$ ,  $26.4^\circ$ ,  $31.3^\circ$ ,  $34.6^\circ$  assigned to V<sub>2</sub>O<sub>5</sub> and at  $16.9^\circ$ ,  $25.3^\circ$ ,  $27.8^\circ$  to FeVO<sub>4</sub> crystallizes arose as the calcined temperature elevated up to 550 and 600 °C (Fig. 1e, f) although the crystalline degree of Fe-V/g-C<sub>3</sub>N<sub>4</sub>-550 was higher than that of Fe-V/g-C<sub>3</sub>N<sub>4</sub>-600 (Fig. SI1). Meanwhile, the (002) plane diffraction of g-C<sub>3</sub>N<sub>4</sub> again appeared at  $2\theta = 27.5^\circ$  for Fe-V/g-C<sub>3</sub>N<sub>4</sub>-550 and Fe-V/g-C<sub>3</sub>N<sub>4</sub>-600, accompanied by stronger and wider peaks observed at  $13.1^\circ$  as well. The stronger and wider peaks for the (100) plane was also due to the strong interaction between Fe or V species and the in-plane structure motif of g-C<sub>3</sub>N<sub>4</sub> at higher

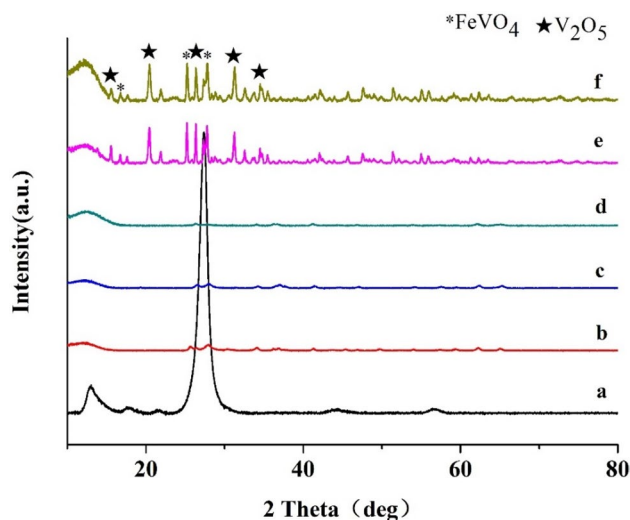


**Fig. 1** XRD patterns of g-C<sub>3</sub>N<sub>4</sub> and Fe-V/g-C<sub>3</sub>N<sub>4</sub>-t at various calcined temperatures. (a) g-C<sub>3</sub>N<sub>4</sub>, (b) Fe-V/g-C<sub>3</sub>N<sub>4</sub>-400, (c) Fe-V/g-C<sub>3</sub>N<sub>4</sub>-450, (d) Fe-V/g-C<sub>3</sub>N<sub>4</sub>-500, (e) Fe-V/g-C<sub>3</sub>N<sub>4</sub>-550, and (f) Fe-V/g-C<sub>3</sub>N<sub>4</sub>-600

calcined temperature. It was clearly that the composites Fe-V/g-C<sub>3</sub>N<sub>4</sub>-550 and Fe-V/g-C<sub>3</sub>N<sub>4</sub>-600 were composed of three crystallizes, FeVO<sub>4</sub>, V<sub>2</sub>O<sub>5</sub> and g-C<sub>3</sub>N<sub>4</sub> with the molar ratio of FeVO<sub>4</sub>:V<sub>2</sub>O<sub>5</sub>:g-C<sub>3</sub>N<sub>4</sub> estimated to be  $\approx 1.6:1:1$  (5.73:3.46:3.57 mmol) for the Fe-V/g-C<sub>3</sub>N<sub>4</sub>-550 sample by the contents of Fe: 19.8% and V: 24.3% in the composite. The determined contents of Fe and V elements by ICP-MS indicated that the amount of the precursor g-C<sub>3</sub>N<sub>4</sub> was obviously reduced from 2.0 to 0.33 g during the preparation of Fe-V/g-C<sub>3</sub>N<sub>4</sub>-550. This reduction of g-C<sub>3</sub>N<sub>4</sub> amount was mainly attributed to the action of Fe species since this reduction was not found during the preparation of VO<sub>x</sub>/g-C<sub>3</sub>N<sub>4</sub> [14]. Usually, Fe(III) or Fe(II) was prone to coordinating to NH<sub>2</sub> groups to form Fe-NH<sub>2</sub> complexes [18]. This interaction between Fe species and -NH<sub>2</sub> in g-C<sub>3</sub>N<sub>4</sub> molecules greatly affected crystallization of g-C<sub>3</sub>N<sub>4</sub>, even caused its decomposition at high calcined temperature. The formation progress of V<sub>2</sub>O<sub>5</sub> and FeVO<sub>4</sub> crystallizes for Fe-V/g-C<sub>3</sub>N<sub>4</sub>-550 and Fe-V/g-C<sub>3</sub>N<sub>4</sub>-600, as well as the decrease in crystalline degree of Fe-V/g-C<sub>3</sub>N<sub>4</sub>-400, Fe-V/g-C<sub>3</sub>N<sub>4</sub>-450 and Fe-V/g-C<sub>3</sub>N<sub>4</sub>-500 could be also observed in SEM images of these samples. As shown in Fig. 2, g-C<sub>3</sub>N<sub>4</sub> presented laminated crystallizes (Fig. 2a) and a part of the laminated crystalline was broken into some pieces when the Fe and V compounds introduced. Moreover, these pieces grew in quantity as the calcined temperature raised from 400 to 500 °C (Fig. 2b-d). Subsequently, the crystalline degree of the composite materials Fe-V/g-C<sub>3</sub>N<sub>4</sub>-550 and Fe-V/g-C<sub>3</sub>N<sub>4</sub>-600 was heightened although the sheet-like crystalline remarkably aggregated, which was in agreement with the results obtained by XRD patterns as shown in Fig. 1d, e.

For further determining the surface composition and structure of the sample Fe-V/g-C<sub>3</sub>N<sub>4</sub>, the SEM-EDX was used to detect the element composition by scanning six different areas, including large sheets and small flakes or pieces as shown in Fig. SI2. The presence of C, N, O, Fe and V lines was confirmed on all these areas, which suggested that V<sub>2</sub>O<sub>5</sub>, FeVO<sub>4</sub> and g-C<sub>3</sub>N<sub>4</sub> crystalline would be uniformly distributed on the Fe-V/g-C<sub>3</sub>N<sub>4</sub>-550 surface, whether on the small flakes or big sheets even though they were too tiny crystals to be observed by SEM. Also, the EDX elemental mapping was applied to elucidate the scattering degree of C, N, O, Fe and V elements on Fe-V/g-C<sub>3</sub>N<sub>4</sub>-550 surface. The mapping results as shown in Fig. 3 presented that the distribution of C, N, O, Fe and V elements was very uniform by highly-dispersed dots. Besides, TEM image of Fe-V/g-C<sub>3</sub>N<sub>4</sub>-550 indicated that the composite material was composed of aggregated globular particles with about 30–50 nm and abundant pores on the surface were clearly observed as white dots (Fig. 4a). Further, a high-resolution TEM image suggested that three lattice fringes for V<sub>2</sub>O<sub>5</sub>, FeVO<sub>4</sub> and g-C<sub>3</sub>N<sub>4</sub> crystalline particles were found with interplanar

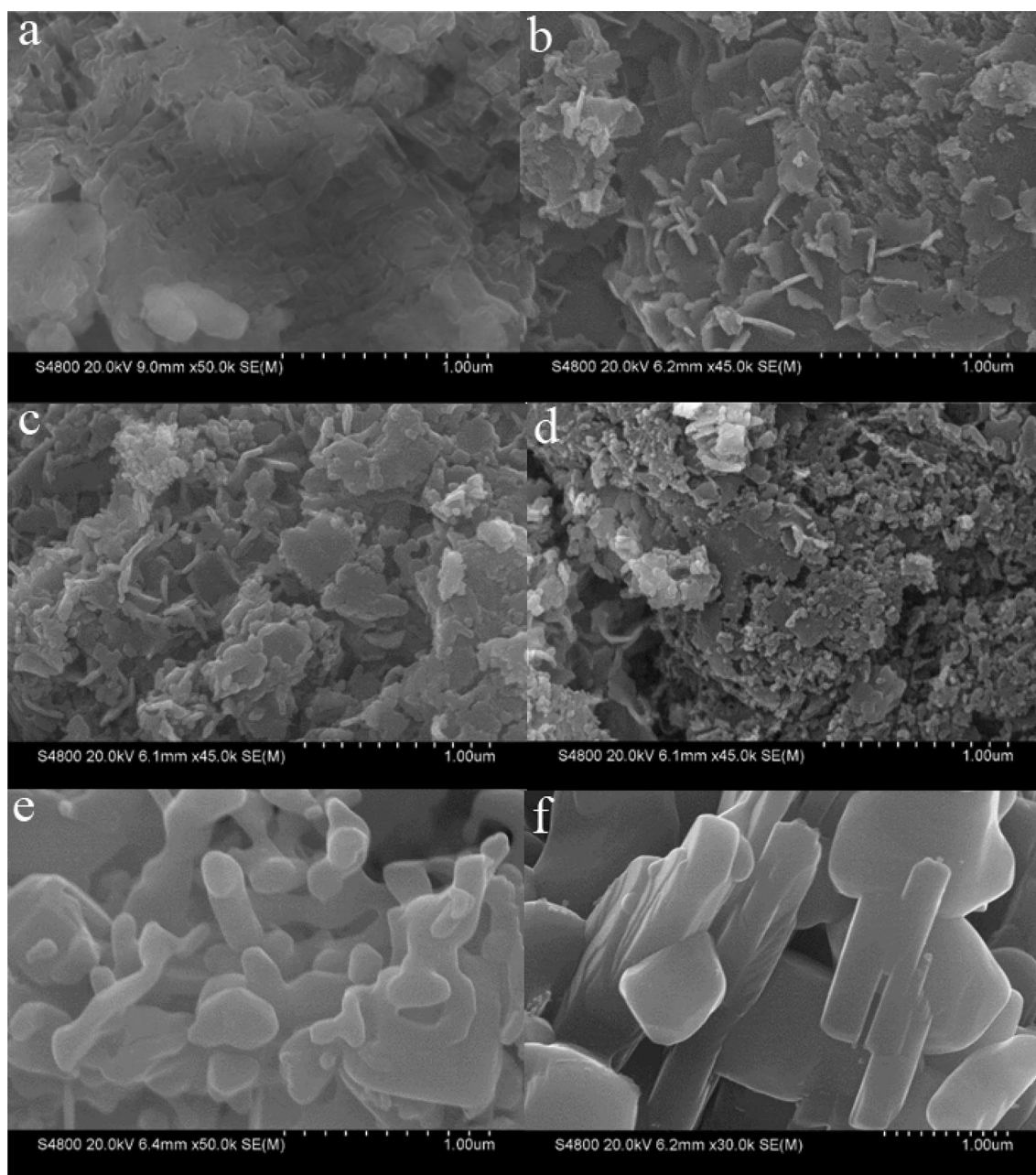


**Fig. 2** SEM images of  $g\text{-C}_3\text{N}_4$  and  $\text{Fe-V/g-C}_3\text{N}_4\text{-t}$ . **a**  $g\text{-C}_3\text{N}_4$ , **b**  $\text{Fe-V/g-C}_3\text{N}_4\text{-400}$ , **c**  $\text{Fe-V/g-C}_3\text{N}_4\text{-450}$ , **d**  $\text{Fe-V/g-C}_3\text{N}_4\text{-500}$ , **e**  $\text{Fe-V/g-C}_3\text{N}_4\text{-550}$ , and **f**  $\text{Fe-V/g-C}_3\text{N}_4\text{-600}$

spacing 0.3314 nm for 330 plane of  $\text{V}_2\text{O}_5$ , 0.4627 nm for 110 plane of  $\text{FeVO}_4$  and 0.3144 nm for 110 plane of  $g\text{-C}_3\text{N}_4$  (Fig. 4b), respectively, validating the existence of these three crystals.

Figure 5 displayed the measurement results of  $\text{N}_2$  adsorption–desorption technique. The adsorption isotherms of  $\text{Fe-V/g-C}_3\text{N}_4\text{-t}$  composites belonged to III type (Fig. 5a). The adsorption capacity at high  $p/p_0$  values was sharply increased for  $\text{Fe-V/g-C}_3\text{N}_4\text{-400}$ ,  $\text{Fe-V/g-C}_3\text{N}_4\text{-450}$ ,  $\text{Fe-V/g-C}_3\text{N}_4\text{-500}$  and  $\text{Fe-V/g-C}_3\text{N}_4\text{-550}$ ,

leading to their higher specific surface areas with 47.4, 51.9, 43.9 and 29.3  $\text{m}^2/\text{g}$ , respectively, as shown in parentheses of Fig. 5. Whereas, the specific surface area of  $\text{Fe-V/g-C}_3\text{N}_4\text{-600}$  (19.3  $\text{m}^2/\text{g}$ ) was slightly larger than that of  $g\text{-C}_3\text{N}_4$  (14.7  $\text{m}^2/\text{g}$ ) due to their similar adsorption isotherms. The higher surface areas of  $\text{Fe-V/g-C}_3\text{N}_4\text{-t}$  were attributed to formation of micro and mesopores owing to decomposition of  $g\text{-C}_3\text{N}_4$  at high temperature. In other words, the precursor  $g\text{-C}_3\text{N}_4$  partly acted as a template agent for the preparation of these porous materials. The

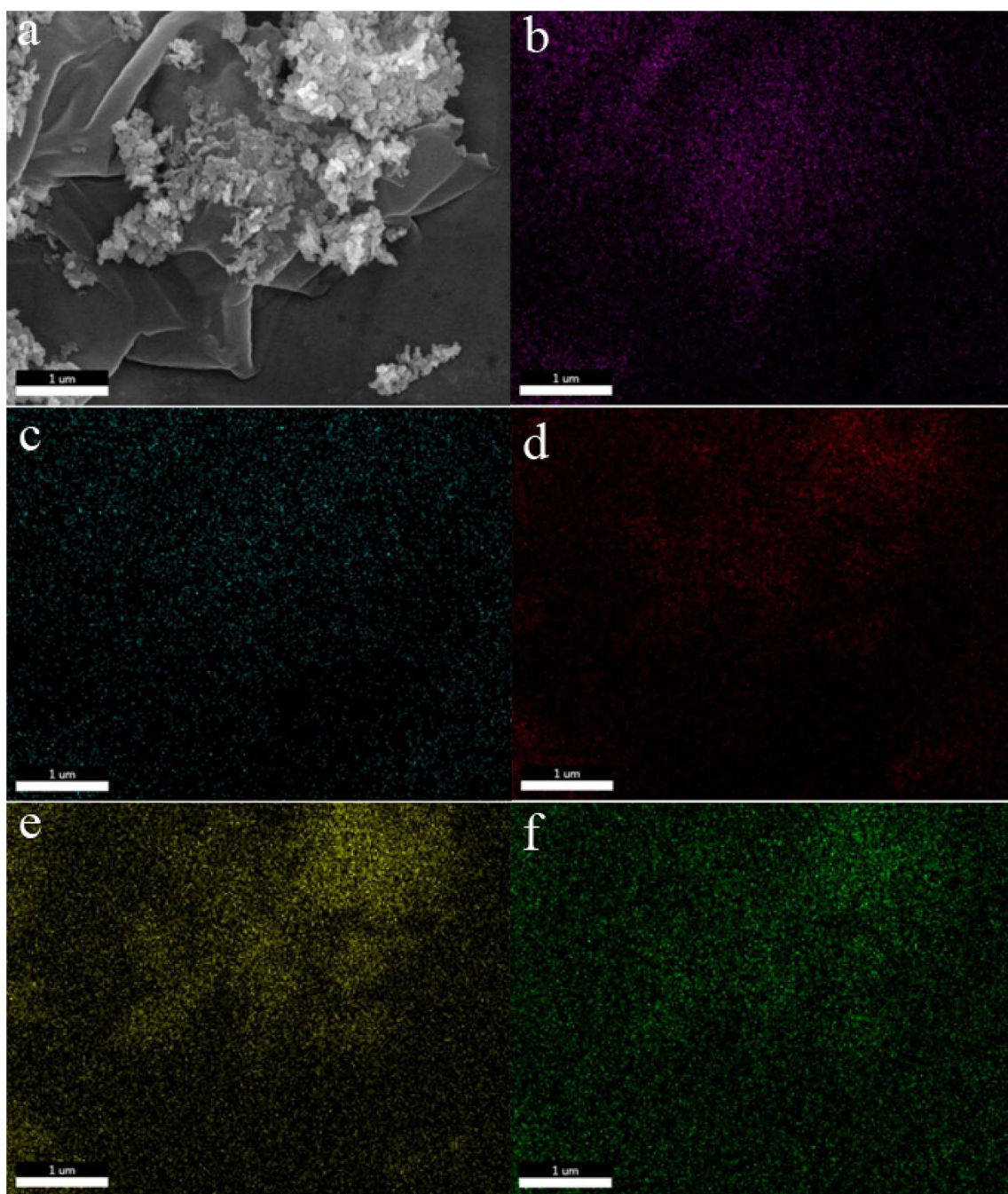


**Fig. 3** EDX elemental mapping of Fe-V/g-C<sub>3</sub>N<sub>4</sub>-550

distribution of pore diameters for the porous materials such as Fe-V/g-C<sub>3</sub>N<sub>4</sub>-450 and Fe-V/g-C<sub>3</sub>N<sub>4</sub>-500, as well as g-C<sub>3</sub>N<sub>4</sub> for comparison, was measured and depicted in Fig. 5b. As compared with g-C<sub>3</sub>N<sub>4</sub>, the pore diameters of Fe-V/g-C<sub>3</sub>N<sub>4</sub>-450 and Fe-V/g-C<sub>3</sub>N<sub>4</sub>-500 shifted from micropore to mesopore direction as a whole, which was the reason that the specific surface areas of the Fe-V/g-C<sub>3</sub>N<sub>4</sub>-450 and Fe-V/g-C<sub>3</sub>N<sub>4</sub>-500 were much more than that of g-C<sub>3</sub>N<sub>4</sub>.

FT-IR spectra of g-C<sub>3</sub>N<sub>4</sub> and Fe-V/g-C<sub>3</sub>N<sub>4</sub>-t prepared at different calcined temperatures were depicted in Fig. 6. As observed in the spectrum of g-C<sub>3</sub>N<sub>4</sub> (Fig. 6a), the broad bands centred at 3432.9 and 3268.2 cm<sup>-1</sup> could be attributed to the stretching vibrational mode of N-H bonds of uncondensed amino groups and the band at 3171.1 cm<sup>-1</sup> was related to the formation of hydrogen bonds in g-C<sub>3</sub>N<sub>4</sub> molecules [19]. The bands from 1252.3 to 1638.0 cm<sup>-1</sup> were likely assigned to the stretching vibrations of the

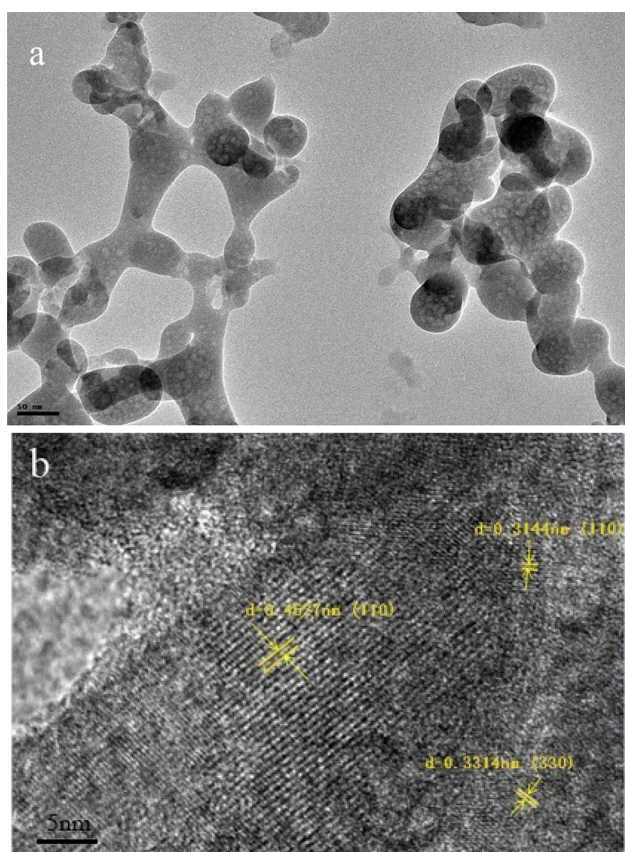


**Fig. 4** TEM (a) and HRTEM (b) of Fe-V/g-C<sub>3</sub>N<sub>4</sub>-550

CN heterocycles [20]. While, the characteristic band at 807.3 cm<sup>-1</sup> corresponded to the typical bending vibration of the triazine unit [21]. As Fe and V species incorporated into g-C<sub>3</sub>N<sub>4</sub>, the feature bands centred at 3268.2 and 3171.1 cm<sup>-1</sup> were obviously decreased for Fe-V/g-C<sub>3</sub>N<sub>4</sub>-400, Fe-V/g-C<sub>3</sub>N<sub>4</sub>-450 and Fe-V/g-C<sub>3</sub>N<sub>4</sub>-500 (Fig. 6b–d), and even they completely disappeared for Fe-V/g-C<sub>3</sub>N<sub>4</sub>-550 and Fe-V/g-C<sub>3</sub>N<sub>4</sub>-600 (Fig. 6e, f). Meanwhile, the bands at 1638.0, 1459.3, 1326.3 and 1252.3 cm<sup>-1</sup>, ascribed to the stretching vibrations of the CN heterocycles, also vanished for Fe-V/g-C<sub>3</sub>N<sub>4</sub>-550 and Fe-V/g-C<sub>3</sub>N<sub>4</sub>-600 samples. The decrease or disappearance of these bands revealed that the interaction between functionalized groups NH<sub>2</sub>- in the g-C<sub>3</sub>N<sub>4</sub> molecules and Fe or V compounds really existed yet during the preparation of these composites, and the interaction was enhanced as the temperature elevated as well. Except for these findings, new bands at 838.7, 915.1, and 960.2 cm<sup>-1</sup> likely assigned to V–O–V linkage, whereas the new bands centred at 991.6 and 1023.0 cm<sup>-1</sup> were clearly found for Fe-V/g-C<sub>3</sub>N<sub>4</sub>-550 and Fe-V/g-C<sub>3</sub>N<sub>4</sub>-600 samples, these two new bands at 991.6 and 1023.0 cm<sup>-1</sup> probably caused by the shift of the stretching vibration of V=O bonds from 1021 cm<sup>-1</sup> due to the strong interaction between VO<sub>x</sub> in V<sub>2</sub>O<sub>5</sub> and FeVO<sub>4</sub> crystallizes and g-C<sub>3</sub>N<sub>4</sub> molecules as

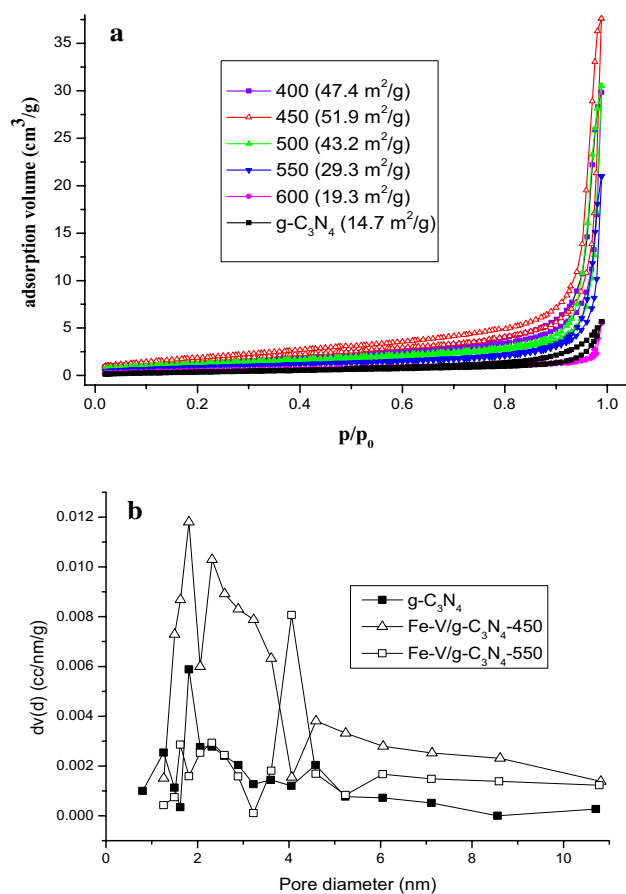


**Fig. 5** Adsorption isotherm (a) and pore diameter distribution (b) of g-C<sub>3</sub>N<sub>4</sub> and Fe-V/g-C<sub>3</sub>N<sub>4</sub>-t (t = 450, 550)

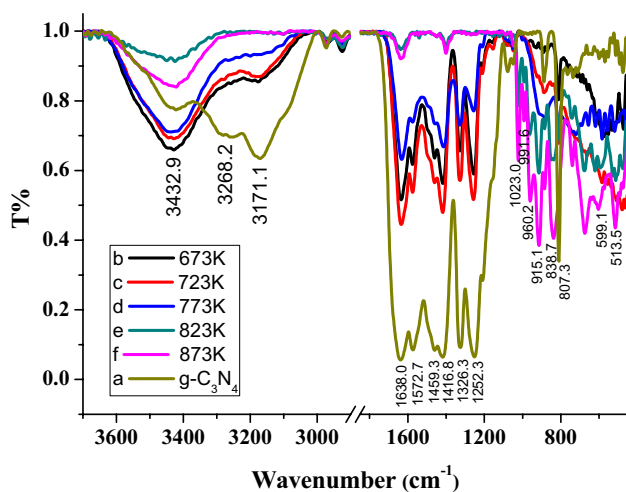


**Fig. 6** FT-IR spectra of g-C<sub>3</sub>N<sub>4</sub> and Fe-V/g-C<sub>3</sub>N<sub>4</sub>-t prepared at various calcined temperature. (a) g-C<sub>3</sub>N<sub>4</sub>, (b) Fe-V/g-C<sub>3</sub>N<sub>4</sub>-400, (c) Fe-V/g-C<sub>3</sub>N<sub>4</sub>-450, (d) Fe-V/g-C<sub>3</sub>N<sub>4</sub>-500, (e) Fe-V/g-C<sub>3</sub>N<sub>4</sub>-550, and (f) Fe-V/g-C<sub>3</sub>N<sub>4</sub>-600

compared with bulk V<sub>2</sub>O<sub>5</sub> molecules [22], that is, existence of V<sub>2</sub>O<sub>5</sub> and FeVO<sub>4</sub> species on the composite materials was surely validated.

X-ray photoelectron spectroscopy (XPS) measurement was conducted to determine the elemental composition and chemical states of the Fe-V/g-C<sub>3</sub>N<sub>4</sub> catalyst. Figure 7a exhibited the presence of C, N, O, Fe and V elements, which confirmed the formation of the Fe-V/g-C<sub>3</sub>N<sub>4</sub> composite

combined with the above XRD, SEM-EDX, FT-IR and HR-TEM. Deconvoluting C 1s spectrum (Fig. 7b), the two peaks centered at 284.5 and 286.7 eV were likely assigned to the graphitic carbon and the sp<sup>2</sup> carbon atoms (N-C=N), respectively [23]. In Fig. 7c, the two signals at 399.8 and 401.6 eV could be ascribed to the sp<sup>2</sup>-hybridized N atom in the thiazine ring and the tertiary nitrogen N-(C)<sub>3</sub>, respectively [24]. Meanwhile, the characteristic peaks at 711.3 and 725.4 eV

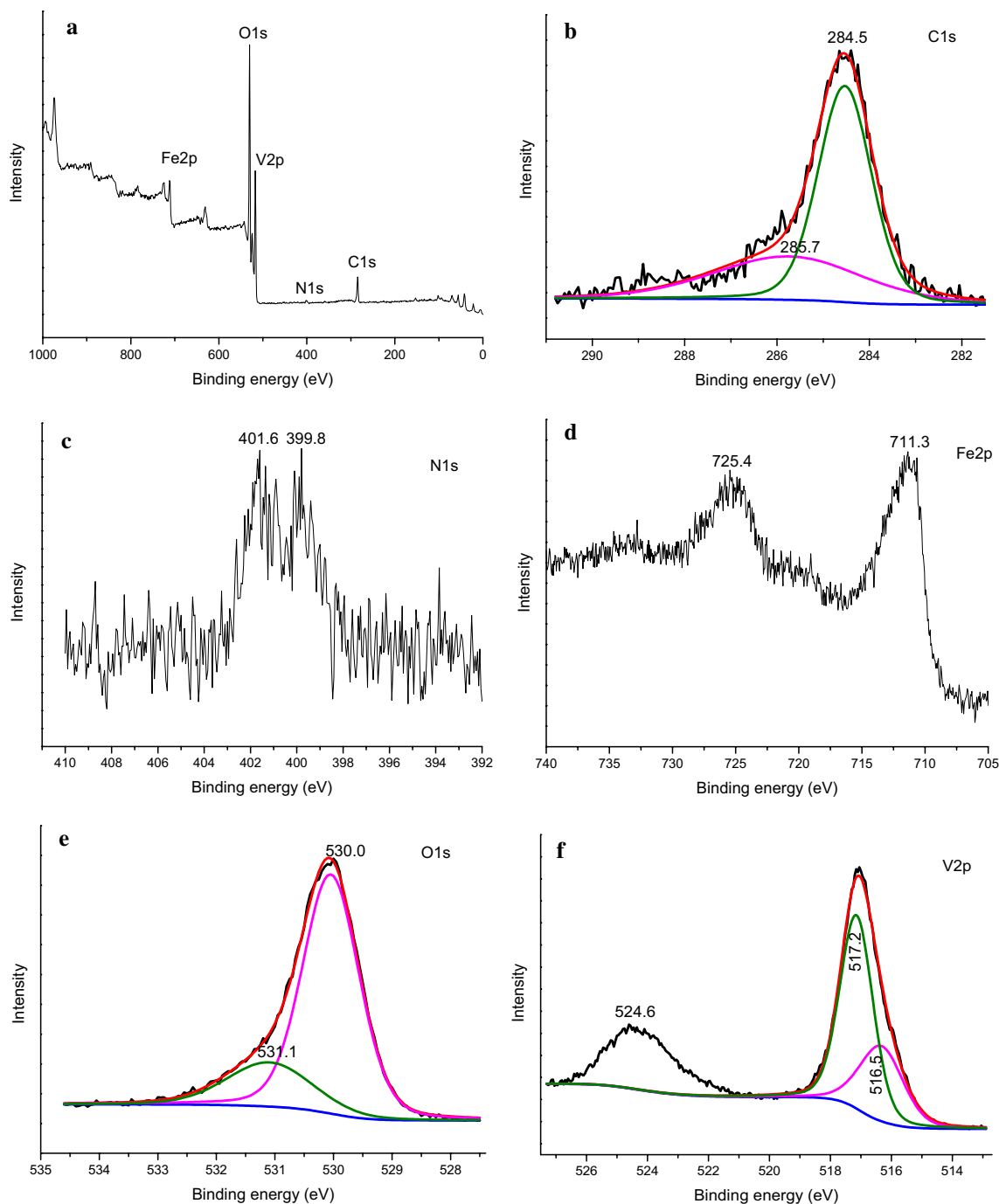


Fig. 7 XPS of Fe-V/g-C<sub>3</sub>N<sub>4</sub>-550 composite

were related to Fe  $2p_{3/2}$  and Fe  $2p_{1/2}$  [25], respectively, as shown in Fig. 7d. Besides, the peaks centered at 530.0 and 531.1 eV in O 1s spectrum of Fig. 7e were assigned to oxygen atoms in  $V_2O_5$  and  $FeVO_4$  species, respectively. Likely, the characteristic peaks at 516.5 and 517.2 eV were attributed to V atoms in  $V_2O_5$  and  $FeVO_4$  species, respectively (Fig. 7f). These findings also demonstrated that the successful formation of Fe–V/g- $C_3N_4$  composite.

### 3.2 Catalytic Activity

The oxidation of methanol conducted in a 100 mL stainless steel autoclave with an electric heater and a mechanical stirrer. The reactants included 20 mL (0.494 mol) of methanol and an initial  $O_2$  pressure of 1 MPa (about 0.0368 mol) at room temperature. If the total 0.531 mol of reactants (methanol +  $O_2$ ) were completely gasified at reaction temperature 175 °C, the total pressure of the reactor would be 19.5 MPa. Actually, the displayed reaction pressure of the oxidation process on the piezometer was about 4.5 MPa, which proved the reaction is liquid-phase oxidation in this case.

It was well known that the surface composition and structure of the catalytic materials strongly depended on the preparation conditions played an important role for the catalytic activity. The dependence of catalytic activity on calcined temperature during the preparation of the catalyst was conducted and the results were presented in Fig. 8. As seen in the figure, the catalytic activity was gradually increased as the calcined temperature raising from 400 to 550 °C, providing from 14.0 to 29.0% conversion of methanol, and then the conversion was sharply decreased to 6.3% for Fe–V/g- $C_3N_4$ -600. Whereas the selectivity to DMM almost remained above 93% for all the Fe–V/g- $C_3N_4$ -t catalysts. This activity order of the catalysts prepared at various calcined

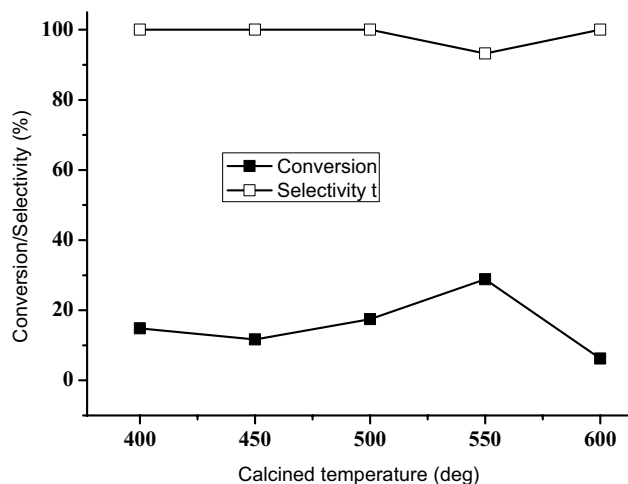


**Fig. 8** The dependence of catalytic activity on the calcined temperature

temperature was indeed relevant to the surface phase composition according to their XRD patterns and FT-IR spectra. As illustrated in Fig. 1, crystallization degree of the composites Fe–V/g- $C_3N_4$ -400, Fe–V/g- $C_3N_4$ -450 and Fe–V/g- $C_3N_4$ -500 was much lower since very weak diffractions of  $V_2O_5$  and  $FeVO_4$  crystalline were observed. When the calcined temperature elevated up to 550 and 600 °C, stronger diffraction peaks of  $V_2O_5$  and  $FeVO_4$  crystallines obviously grew. It was worthy to note that the crystallinity of  $V_2O_5$ ,  $FeVO_4$  and g- $C_3N_4$  in Fe–V/g- $C_3N_4$ -550 was higher than that in Fe–V/g- $C_3N_4$ -600 (Fig. S11). These findings suggested that the redox active sites that arose from the crystalline  $V_2O_5$  or  $FeVO_4$  on the surface of the catalyst were vital for methanol oxidation because the first step of methanol oxidation to formaldehyde is the rate determining one [26]. Especially, the formation of formaldehyde occurred via the transfer of an H atom of a methoxy group to the O atom of the V=O group [27]. As a result, the V=O groups in  $V_2O_5$  and  $FeVO_4$  crystallizes was surely confirmed to act as active sites for methanol oxidation to DMM. Therefore, the Fe–V/g- $C_3N_4$ -550 catalyst with remarkable V=O groups in high crystallization degree of  $V_2O_5$  and  $FeVO_4$  crystallizes, evidently observed in FT-IR spectra, demonstrated higher catalytic activity as compared with Fe–V/g- $C_3N_4$ -400, Fe–V/g- $C_3N_4$ -450 and Fe–V/g- $C_3N_4$ -500, as well as Fe–V/g- $C_3N_4$ -600 catalysts even though Fe–V/g- $C_3N_4$ -400, Fe–V/g- $C_3N_4$ -450 and Fe–V/g- $C_3N_4$ -500 had much higher specific surface areas than the former. In contrast, the low specific surface area and crystalline degree was the reason that the Fe–V/g- $C_3N_4$ -600 catalyst provided lower catalytic activity.

Figure 9 exhibited the dependence of the catalytic activity on initial pressure of oxygen gas. As the initial pressure of  $O_2$  increased, the conversion of methanol was gradually promoted, showing up to about 29.0% conversion at the initial pressure of 1.0 MPa, and then the conversion slightly raised

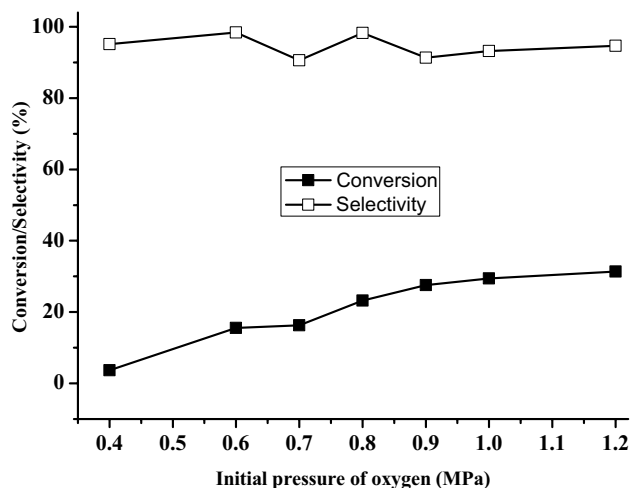


**Fig. 9** The effect of  $O_2$  initial pressure on the catalytic activity

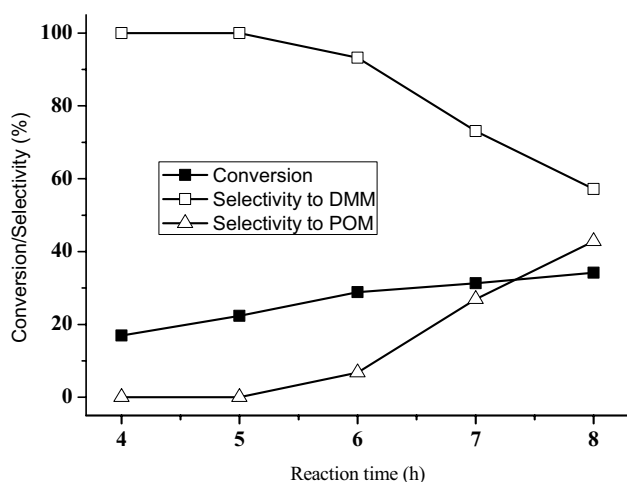


**Fig. 10** The dependence of the catalytic activity on reaction time

as the pressure elevated to 1.2 MPa. At the same time, the selectivity remained above 90.0% in all range of the initial pressure. According to the stoichiometric reaction equation, the O<sub>2</sub> pressure arising surely promoted the surface conversion of methanol. Actually, about 30% conversion of methanol would expend 0.148 mol of methanol and 0.0247 mol of O<sub>2</sub>, while the amount of O<sub>2</sub> approached to 0.67 MPa of initial pressure. Thus, 1.0 MPa of O<sub>2</sub> pressure was enough for the methanol oxidation in this case.

The catalytic activity was remarkably increased as the reaction time prolonged from 4 to 6 h (Fig. 10), and accompanied by the selectivity to DMM decreasing from ca. 100% at 4–5 h to 93.3% at 6 h. Further, the selectivity to DMM was sharply decreased from 93.3 to 57.2% and the conversion was slightly increased up to 34.2% as the reaction time continuously expanded from 6 to 8 h. The deep decrease of the selectivity to DMM was validated to be related to oligomerization of the product DMM into poly(oxymethylene) dimethyl ether (POM). When the reaction completed, the reaction mixture was distilled to remove unreacted methanol and product DMM. The remainder obtained by washed and dried was confirmed to be POM by <sup>13</sup>C NMR and <sup>1</sup>H NMR spectra as shown in Fig. SI3. Moreover, the further detection and analysis exhibited that the obtained POM was identified to be CH<sub>3</sub>(OCH<sub>2</sub>)<sub>8–10</sub>OCH<sub>3</sub> by GC–MS. As a result, the tuneable synthesis of DMM and POM was realized by controlling the reaction time. That is, the POM was obtained as main product when prolonged reaction time > 8 h, and DMM was as main product at reaction time of 6 h, however, the selectivity to DMM and POM was all about 99.0% in any case.

The effect of reaction temperature on the methanol oxidation was performed and the results was demonstrated in Fig. 11. The conversion was smoothly increased as the temperature raising from 160 to 175 °C, and then the conversion

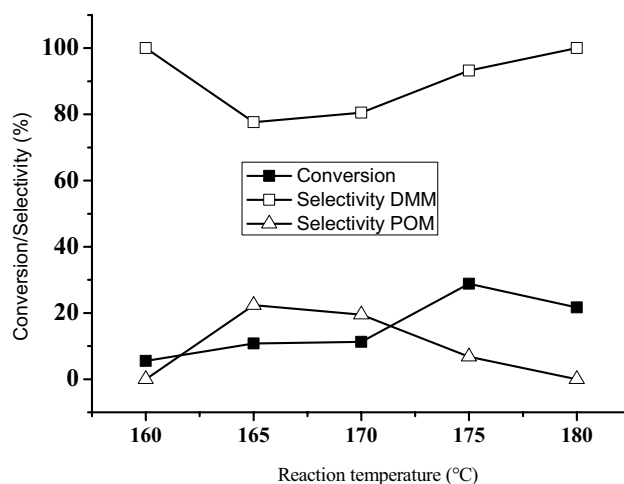
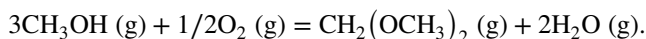
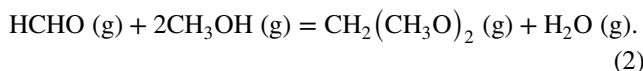


**Fig. 11** The dependence of the catalytic activity on reaction temperature

was decreased as the temperature continuously raising to 180 °C. Besides, the selectivity to DMM reached at ca. 100% at temperature of 160 °C and reduced to about 80% with 20% POM at 165 °C. Thereafter, the selectivity to DMM again raised to ca. 100% at 180 °C. This phenomenon is likely related to the reaction thermodynamics. It was known that the reaction equation of methanol oxidation to DMM is shown in the following:



This includes two reactions to be completed, one is the oxidation of methanol to FM; and the other is the condensation of methanol with FM to generate DMM.



According to the thermodynamics data of  $\Delta G_f^\theta$ ,  $\Delta H_f^\theta$  and  $C_{p,m}$ ,  $\Delta_r G_1^\theta(T)$  and  $\Delta_r G_2^\theta(T)$  for Reactions (1) and (2), respectively, were calculated and the plots of  $\Delta_r G_1^\theta(T)$  and  $\Delta_r G_2^\theta(T)$  versus reaction temperature were demonstrated in Fig. 12a. Evidently, the  $\Delta_r G_2^\theta$  positively shifted as the reaction temperature raising, which makes driving force for the Reaction (2) be changed to be weaker, leading to the decrease in the reaction trend at high temperature. Whereas,  $\Delta_r G_1^\theta$  was reduced as the temperature raising. The temperature elevating is thus disadvantageous for the Reaction (2) forming DMM from the view point of the reaction thermodynamics, which led to the low conversion as the reaction temperature increased to 180 °C in this case. On the other hand, the changes of  $\Delta_r G_{\text{pol}}^\theta$  for polymerization reaction

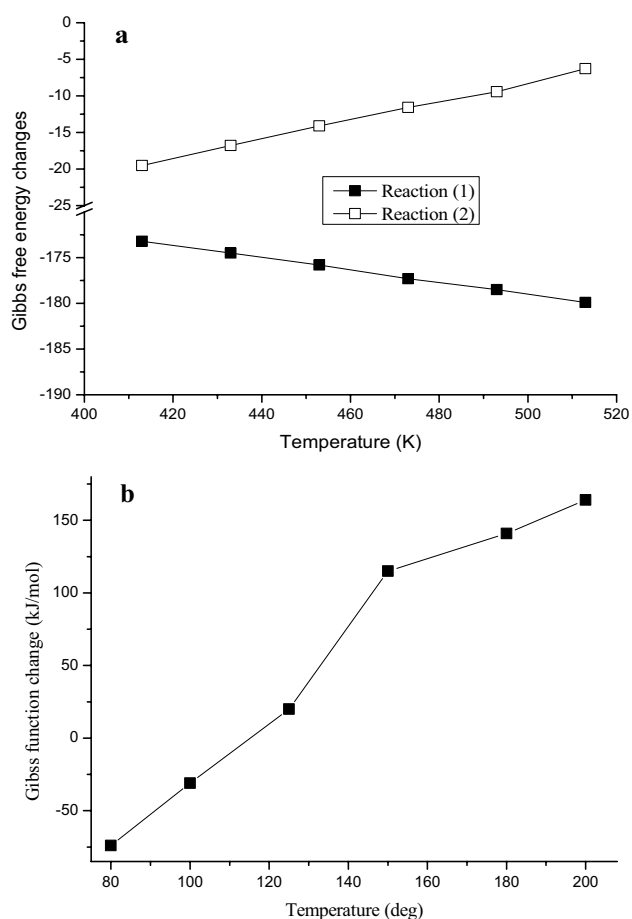


Fig. 12 Dependence of  $\Delta_r G_T^\ominus$  on the reaction temperature

to POM with the temperature was also depicted in Fig. 12b [28]. The  $\Delta_r G_{\text{pol}}^\ominus$  values was changed to be more positive above 120 to 150 °C, also it was increased with the temperature rising from 150 to 200 °C, which would inhibit the polymerization carried out in view point of the thermodynamics, inevitably causing the decrease of the selectivity to POM.

### 3.3 The Reusability and Stability of the Catalyst

In order to estimate the application prospect of the catalyst in industry, the reusability and/or lifetime of the catalyst were explored in batch and fixed-bed reactor. The results were depicted in Fig. 13. For the batch reaction, the catalyst was recovered, dried and reused in the next run under the same reaction conditions. As shown in Fig. 13a, the catalytic activity of the catalyst Fe-V/g-C<sub>3</sub>N<sub>4</sub>-550 was almost unaffected even at the third run and the lower activity for the fourth run was likely ascribed to the weight loss during the recovery of the catalyst. This indicated that the catalyst had a good reusability in batch reaction. Besides, the catalytic activity was increased at the initial stage from

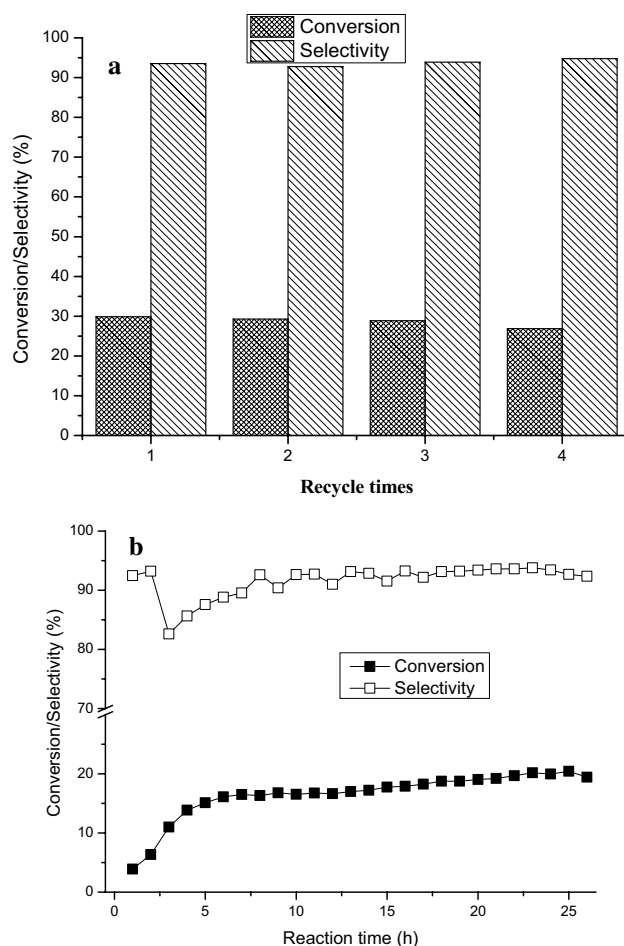


Fig. 13 Reusability (a) and stability (b) of the catalyst. a Batch reaction and b fixed-bed reaction

1 to 5 h, exhibiting the conversion 15.5% at 5 h in fixed-bed reactor (Fig. 13b). Subsequently, the conversion was gradually increased up to about 19.0% at 17 h, followed by achieving 20.4% at 25 h and 19.4% at 26 h. This finding also revealed that the catalyst Fe-V/g-C<sub>3</sub>N<sub>4</sub>-550 was much more stable than the reported V/g-C<sub>3</sub>N<sub>4</sub> catalyst [14], that is, the introducing Fe species into V/g-C<sub>3</sub>N<sub>4</sub> catalyst could greatly enhance the stability of the catalyst for selective oxidation of methanol.

## 4 Conclusions

A composite material Fe-V/g-C<sub>3</sub>N<sub>4</sub> was designed and prepared by impregnation. Its characterization exhibited that the composite was composed of V<sub>2</sub>O<sub>5</sub>, FeVO<sub>4</sub> and g-C<sub>3</sub>N<sub>4</sub> crystalline and possessed higher specific surface areas. The composite displayed high catalytic activity and selectivity for liquid-phase selective oxidation of methanol. This high activity was surely ascribed to V=O groups in V<sub>2</sub>O<sub>5</sub> and

FeVO<sub>4</sub> crystalline, which served as active sites on the catalyst surface. Besides, the tuneable synthesis of DMM and POM was realized by controlling the various reaction time. The composite catalyst possessed excellent reusability and lifetime for the oxidation reaction, which suggested that it has a potential application prospect in industry.

**Acknowledgements** We make a great acknowledgment for the financial support of this work by the National Natural Science Foundation of China (No. 21671050).

## References

1. Thavornprasert K, Capron M, Jalowiecki-Duhamel L, Dumeignil F (2016) *Catal Sci Technol* 6:958
2. Sun Q, Auroux A, Shen J (2006) *J Catal* 244:1
3. Zhang Y, Zhou W, Ma J, Xie M, Wang R (1998) *Nat Gas Chem Ind* 23:22 (in Chinese)
4. Zhao H, Bennici S, Shen J, Auroux A (2010) *J Catal* 272:176
5. Burger J, Siegert M, Ströfer E, Hasse H (2010) *Fuel* 89:3315
6. Satoh S, Tanigawa Y (2002) US Patent, 6,379,507
7. Yuan Y, Shido T, Iwasawa Y (2000) *Chem Commun* 1421
8. Yu H, Zeng K, Fu XB, Zhang Y, Peng F, Wang HJ, Yang J (2008) *J Phys Chem C* 112:11875
9. Chen S, Meng YL, Zhao YJ, Ma XB, Gong JL (2013) *AIChE J* 59:2587
10. Yuan YZ, Liu HC, Imoto H, Shido T, Iwasawa Y (2000) *Chem Lett* 29:674
11. Lu X, Qin Z, Dong M, Zhu H, Wan G, Zhao Y, Fan W, Wang J (2011) *Fuel* 90:1335
12. Zhang QD, Tan YS, Yang CH, Han YZ (2007) *J Mol Catal A* 263:149
13. Tao M, Wang H, Lu B, Zhao J, Cai Q (2017) *N J Chem* 41:8370
14. Ma H, Wang H, Lu B, Zhao J, Cai Q (2019) *Mol Catal* 469:48
15. Li M, Long Y, Deng Z, Zhang H, Yang X, Wang G (2015) *Catal Commun* 68:46
16. Ayers T, Turk R, Lane C, Goins J, Jameson D, Slattery SJ (2004) *Inorg Chim Acta* 357:202
17. Martin DJ, Qiu KP, Shevlin SA, Handoko AD, Chen XW, Guo ZX, Tang JW (2014) *Angew Chem Int Ed* 53:9240
18. He YM, Zhang LH, Teng BT, Fan MH (2015) *Environ Sci Technol* 49:649
19. Rong GB, Zhu SZ (2002) Structure determination of organic compounds, table of spectral data. Press of East China University of Science and Technology, Shanghai
20. Li KX, Zeng ZX, Yan LS, Luo SL, Luo XB, Huo MX, Guo YH (2015) *Appl Catal B* 165:428
21. Zhu Z, Lu ZY, Wang DD, Tang X, Yan YS, Shi WD, Wang YS, Gao NL, Yao X, Dong HJ (2016) *Appl Catal B* 182:115
22. Barbero BP, Cadus LE (2003) *Appl Catal A* 244:235
23. Li YF, Fang L, Jin RX, Yang Y, Fang X, Xing Y, Song SY (2015) *Nanoscale* 7:758
24. Cheng NY, Tian JQ, Liu Q, Ge CJ, Qusti AH, Asiri AM, Al-Youbi AO, Sun XP (2013) *ACS Appl Mater Interfaces* 5:6815
25. He HK, Gao C (2010) *ACS Appl Mater Interfaces* 2:3201
26. Tatibouët JM (1997) *Appl Catal A* 148:213
27. Kaichev VV, Popova GY, Chesalov YA, Saraev AA, Zemlyanov DY, Beloshapkin SA, Knop-Gericke A, Schlögl R, Andrushkevich TV, Bukhtiyarov VI (2014) *J Catal* 311:59
28. Zhang X, Wu P, Jiang Z, Gao X, Liu T, Hu Y (2015) *Chem Eng* 43:39 (in Chinese)

**Publisher's Note** Springer Nature remains neutral with regard to jurisdictional claims in published maps and institutional affiliations.